J Nanopart Res (2016) 18:99
DOI 10.1007/s11051-016-3405-2

RESEARCH PAPER

Oleate coating of iron oxide nanoparticles in aqueous systems: the role of temperature and surfactant concentration

Hans-Christian Roth · Sebastian Schwaminger · Paula Fraga García · Jonathan Ritscher · Sonja Berensmeier

Received: 2 December 2015 / Accepted: 25 March 2016 / Published online: 6 April 2016

Abstract Coating magnetic nanoparticles (MNPs) with sodium oleate (SO) is known to be an excellent method to create biocompatible, stable colloids with a narrow size distribution. However, the mechanism of oleate adsorption on the MNP surface in aqueous systems, as well as its influence on colloidal stability, is not yet fully understood. In this context, we present here a physico-chemical study to provide a deeper understanding of surfactant interaction mechanisms with nanoparticles. We examined the effect of temperature and the SO/MNP ratio (w/w) on the adsorption process in water and observed the existence of a maximum for the adsorbed oleate amount at lower temperatures, whereas at higher temperatures, the isotherm can be adapted to the Langmuir model with constant capacity after saturation. The oleate load on the MNP surface was quantified using reversed-phase high-performance liquid chromatography measurements of samples in solution. The thermogravimetric analyses of the solid residues together with infrared spectroscopy analyses indicate a bilayer-similar structure at the MNP/water interface even for low oleate loads. The oleate interacts with the iron oxide surface through a bidentate coordination of the carboxyl group. Zeta potential measurements demonstrate the high stability of the coated system. The maximal oleate load per unit mass of MNPs reaches approximately 0.35 $g_{oleate}\ g_{MNP}^{-1}$.

Keywords Magnetic nanoparticles · Iron oxide · Oleate · Colloidal stability · Adsorption isotherms

Electronic supplementary material The online version of this article (doi:10.1007/s11051-016-3405-2) contains supplementary material, which is available to authorized users.

H.-C. Roth · S. Schwaminger · P. Fraga García · J. Ritscher · S. Berensmeier (✉)
Bioseparation Engineering Group, Technische Universität München, Boltzmannstraße 15, 85748 Garching, Germany
e-mail: s.berensmeier@tum.de

Introduction

Over the last few decades, magnetic nanoparticles (MNPs) from iron oxides have been a focus of research due to their wide range of application. Their physical, chemical, and especially magnetic properties make them outstanding materials for a variety of research fields (Berensmeier 2006; Brandt and Balducci 2013; Bao et al. 2016). Therefore, the demand for MNPs with controlled properties has resulted in the development of numerous synthesis methods (Reddy et al. 2012; Laurent et al. 2008; Chin and Yaacob 2007; Park et al. 2004). However, one of the well-established synthesis routes for the controlled preparation of a large amount of superparamagnetic MNPs remains the chemical co-precipitation of iron salts in an alkaline environment (Martínez-Mera et al. 2007; Khalafalla and Reimers 1980). Most applications,

though, require a fine and homogenous dispersion of the MNPs in a variety of polar and nonpolar liquids. Particularly in biotechnological and medical applications, the focus lies on aqueous dispersions, where untreated MNPs tend to form aggregates in the range of 100–1000 nm, due to magnetic dipole interactions and van der Waal's forces (Kim et al. 2001). In addition to steric stabilization with natural and synthetic polymers, electrostatic stabilization is commonly used in order to maintain a stable MNP dispersion with a narrow size distribution. Some reviews have summarized strategies for surface modification of nanofluids towards better stability (Ramimoghadam et al. 2015a). As a result of their biocompatibility and nontoxicity, fatty acids are among the most interesting coating agents on MNPs for both stabilization in aqueous (Wang et al. 2003; 2007b) and nonpolar liquids (Rudolph et al. 2012; Zhang et al. 2006; Korolev et al. 2004). The fatty acids act as surface active agents with a polar headgroup and a hydrophobic tail. In the case of aqueous systems, they build a water impermeable bilayer around the MNP: in the inner layer, the carboxylic head group adsorbs on the MNP surface, whereas the nonpolar tail group orients towards the solvent. In the outer layer, the nonpolar tail group of dissolved fatty acids interacts with the nonpolar tail groups of adsorbed fatty acids, thus creating a double layer on the MNP surface with carboxylic acid head groups facing towards the solvent (Wang et al. 2007b). Fatty acids with different chain lengths and carbon hydrate saturation levels have been studied with regard to their surface interaction with superparamagnetic iron oxide nanoparticles and their effect on stabilization. As a result of such studies, oleic acid and its salt, sodium oleate (SO), seem to be the most promising candidates for a highly stabilized system. While the adsorption of SO on MNP has been discussed for several nonpolar liquids and temperatures (Balmasova et al. 2010; Korolev et al. 2002, 2009), detailed studies of adsorption isotherms in aqueous systems have rarely been covered (Roonasi and Holmgren 2009; Zhou et al. 2007). A systematic investigation of the influence of coating parameters on the physical and chemical nature of the lipid double layer and the resulting colloidal stability are still necessary. Kulkarni and Somasundaran carried out intensive research for hematite systems (Kulkarni and Somasundaran 1980). Scamehorn et al. examined the adsorption of surfactants on iron oxide surfaces from aqueous solutions and indicated the four regions in the adsorption isotherms as well as corresponding potential mechanisms of adsorption (Scamehorn et al. 1982). Although there are some general studies in the literature on this topic (Paria and Khilar 2004), a clear description has not yet been presented and fundamental questions regarding the organization of the surfactant at the interphase remain open. Although some authors support the theory that adsorption occurs as a monolayer (Roonasi and Holmgren 2009), our results support the existence of a bilayer-similar structure even for very low surface coverage with oleate.

In the present study, we systematically investigate the influence of different temperatures on the oleate adsorption at the surface of MNPs in aqueous media. In order to prepare isotherms of adsorption, the coating procedure is operated stepwise in a well-defined and controlled reaction setup. To understand nanoparticle stabilization mechanisms and, more specifically, the interplay between the different interaction forms in the system (surfactant-nanoparticle surface, surfactant–surfactant, surfactant-solvent), more reliable characterization methods are required in solution. We apply reversed-phase high-performance liquid chromatography (RP-HPLC) to quantify the oleate content in the reaction supernatants. This method is known in other application fields, such as bio-fuels (Holčapek et al. 1999) and bio-medicals (Norlén et al. 1998), but as far as we know, there do not appear to be similar physicochemical studies which quantify the fatty acids using RP-HPLC. Common analytics in this field are thermogravimetric analysis (TGA) (Korolev et al. 2002; Wang et al. 2007a; Yan et al. 2009) and Fourier transform infrared spectroscopy (FT-IR) (Bloemen et al. 2012; Chen et al. 2014; Ramos-González et al. 2012); both analyze the solid residues after supernatant removal and a subsequent drying process. However, the analysis in solution is of special importance to avoid alterations in the sample structure. Furthermore, RP-HPLC has the advantage of a high analytical sensitivity and automatized sampling, the latter of which results in high throughput measurements. TGA measurements enabled us to demonstrate the existence of an oleate bilayer. Furthermore, we characterized the interaction of the oleate with the MNP surface using FT-IR spectroscopy and determined changes in the surface charge of the shear plane

around the particles by zeta potential analysis. This fundamental study aims to understand a system oriented towards large-scale application. Therefore, and due to the very high price of sodium oleate, we chose a technical grade substance for the experiments and investigated its ability to stabilize magnetic nanoparticles under conditions relevant for industrial goals.

Experimental

Materials

Ferric chloride hexahydrate ($FeCl_3$) (98 %) and sodium hydroxide (NaOH) (97 %) were purchased from AppliChem GmbH, Germany. Ferrous chloride tetrahydrate ($FeCl_2$) (98 %) was obtained from Bernd Kraft GmbH, Germany. Sodium oleate (SO) (technical grade, >90 %) and acetonitrile (ACN) (HPLC grade) were provided by J. T. Baker, Germany and SO (>99 %) from Sigma Aldrich Corporation, Germany. Acetic acid (99.7 %), L-(+) ascorbic acid (>99 %), hydrochloric acid (HCl) (37 %), trifluoroacetic acid (TFA) (99.9 %) and 1,10-*o*-phenanthroline hydrochloride monohydrate (>99 %) were ordered from Carl Roth GmbH & Co. KG, Germany. Fatty acid methyl ester marine oil mix (FAME-Mix) was purchased from Restek GmbH, Germany. All chemicals were used as purchased without any further purification. Aqueous solutions were prepared with degassed and deionized water (dd-H_2O) in all experiments. The impurities of the oleate were analyzed using GC–MS. They are mainly C16 and C14 fatty acids: palmitic acid (C16) and myristic acid (C14) as well as some C18 fatty acids (vaccenic acid and oleic acid).

Methods

Synthesis of MNPs

Highly dispersed magnetic nanoparticles were synthesized as previously described (Roth et al. 2015). Process conditions, such as temperature, pH value, dosing, and stirring rate, were controlled and monitored by the fully automated OptiMax™ synthesis station (Mettler-Toledo GmbH, Germany). In a typical synthesis protocol, 40 g $FeCl_2$ and 108 g $FeCl_3$ were each dissolved in 100 mL dd-H_2O. The iron salt solutions were mixed in a nitrogen atmosphere and added to 800 mL of 1.8 M NaOH solution at a dosing rate of 150 mL min^{-1}. Throughout the whole synthesis, the reaction solution was stirred under a steady flow of nitrogen in order to prevent oxidation. The addition of the iron salt solution to the NaOH solution instantly resulted in the formation of a black precipitate, which was washed with dd-H_2O in order to remove residual NaOH and sodium chloride several times. The washing procedure was performed until the solution conductivity dropped below 200 μS cm^{-1}.

Oleate adsorption on MNPs

The adsorption equilibria of SO on MNP were investigated at the temperatures 4, 25, and 60 °C. Therefore, 12 samples with increasing weight ratios of SO to MNP were prepared for each temperature. A detailed summary of the reaction conditions is shown in Table 1. All experiments were reproduced as triplicates in 2-mL reaction vessels and a solid content of 4.3 mg_{MNP} mL^{-1}. Adsorption time was adjusted to 3 h in the Eppendorf Thermomixer® comfort (Eppendorf AG, Germany) at a mixing speed of 1200 rpm. According to kinetic studies by Roonasi et al., this incubation time should be sufficient to achieve adsorption equilibrium (Roonasi et al. 2010).

Table 1 Reaction conditions for oleate adsorption isotherms on MNPs

Sample			SO/MNP wt-ratio g_{SO} g_{MNP}^{-1}
4 °C	25 °C	60 °C	
T4_01	T25_01	T60_01	0.02
T4_02	T25_02	T60_02	0.04
T4_03	T25_03	T60_03	0.10
T4_04	T25_04	T60_04	0.15
T4_05	T25_05	T60_05	0.20
T4_06	T25_06	T60_06	0.25
T4_07	T25_07	T60_07	0.30
T4_08	T25_08	T60_08	0.35
T4_09	T25_09	T60_09	0.40
T4_10	T25_10	T60_10	0.60
T4_11	T25_11	T60_11	1.00
T4_12	T25_12	T60_12	1.40

Subsequently, the magnetic content was separated from the liquid medium using NdFeB magnets; the temperature was kept constant with regard to the value of the adsorption experiment. Samples from the clear supernatant were collected for RP-HPLC analytics. The residues were washed twice with dd-H_2O to avoid falsification of analytics with dissolved SO. The oleate mass loss due to the two wash steps was <5 % for all samples. One part of the samples was stored in a nitrogen atmosphere for zeta potential measurements, while the other part of the colloids was lyophilized with an ALPHA 1-2 LDplus (Martin Christ Gefriertrocknungsanlagen, Germany) and stored in a nitrogen atmosphere at –20 °C for TGA and FT-IR analytics.

Analytics

Physico-chemical characterization of MNPs

Quantitative iron analysis was performed spectrophotometrically to determine the solid content in the iron oxide suspensions (Schilt 1969). A specific volume of the MNP suspension was treated with 37 % HCl in order to dissolve the solid MNP content. Subsequently, the acidic iron solution was diluted with dd-H_2O in a ratio of 1:14.3. Then, 40 µL of the diluted iron solution was buffered at pH 4.5 with a sodium acetate buffer and treated with ascorbic acid for 10 min to reduce all iron ions to Fe^{2+}. The addition of 1,10-*o*-phenanthroline solution resulted in the formation of an orange/red chelate complex. Sample analysis was performed at a wavelength of 510 nm with the Infinite® 200 Pro (Tecan Group Ltd., Switzerland) spectrophotometer. The concentrations of MNP per unit volume were indirectly calculated from the related iron concentrations, assuming that all iron oxides were composed of Fe_3O_4, as previously demonstrated by Roth et al. (2015). The crystal structure and phase purity of the precipitates were confirmed using powder X-ray diffraction (XRD) and Raman spectroscopy in the same manner as in previous studies (Roth et al. 2015) (Fig. S2). Gas adsorption isotherms according to the BET (Brunauer–Emmett–Teller) were accomplished as described elsewhere (Schwaminger et al. 2015).

RP-HPLC

A quantitative analysis of SO in aqueous media was conducted with reversed-phase HPLC (RP-HPLC) using a Synergi™ 4 µm Polar-RP 80 Å, LC column (Phenomenex Inc., USA) in an Agilent 1100 Series System (Agilent Technologies Inc., USA). The mobile phase consisted of 20 mM TFA in 80 % (v/v) ACN aqueous solution and was adjusted to a flow rate of 0.2 mL min^{-1}. The detection of components was performed spectrophotometrically via UV-absorption at 205 nm. In order to identify the oleate peak and detect impurities, peak fractions from RP-HPLC were collected and methylated according to the method described by Griffiths et al. (2010). Methylated samples were analyzed using the gas chromatography system GC Trace Ultra (Thermo Fisher Scientific Inc., USA) in combination with the mass spectrometer MS DSQ2 (Thermo Fisher Scientific Inc., USA). The oleate peak was identified using the FAME-Mix as the external standard. Peak areas from RP-HPLC were used to quantify the oleate content in the samples.

Infrared spectroscopy

Lyophilized samples of coated MNPs were characterized by FT-IR spectroscopy. A Bruker Optics Tensor 27 spectrometer (Bruker Optics, Ettlingen, Germany), equipped with a Bruker Optics Platinum ATR accessory (diamond crystal with single reflection) and with a room temperature deuterated triglycine sulfate (RT-DTGS) detector, was applied for all experiments. Each sample was recorded twice against air background (from 4000 to 400 cm^{-1} with a spectral resolution of 4 cm^{-1}), changing the position between two measurements on the ATR crystal, and averaged 64 times. For all spectra an atmospheric compensation, an ATR correction (experimental ATR correction factor for magnetite 1.91) and a concave rubber band baseline correction were applied with the software OPUS 7.2.

Thermogravimetric analysis (TGA)

The adsorption behavior of oleate molecules on MNPs was also determined gravimetrically from lyophilized samples using the simultaneous thermal analysis system STA 449C Jupiter (Netzsch Gerätebau GmbH, Germany). The weight loss and the heat transfer were recorded at a heat rate of 10 K min^{-1} (303–1173 K) in a nitrogen atmosphere. The gas phase was analyzed employing a mass spectrometry system QMS 403 Aeolos (Netzsch Gerätebau, Germany). Mass-to-

charge ratios were recorded at m z^{-1} = 41, 43, 44, 55, 69, 83, and 97, known to be characteristic of the thermal decomposition of oleic acid.

Zeta potential

The change in zeta potential due to adsorbed oleate molecules on the MNP surface was monitored from pH 10 to pH 3 with a Delsa™ Nano C in combination with the Flow Cell and the Delsa™ Nano AT (Beckman Coulter Inc., USA) where 0.1 NaOH and 0.1 HCl were used as titrants.

Results and discussion

Adsorption isotherms

In order to obtain deeper insight into the adsorption mechanisms of oleate on MNP and the parameters influencing this process, coating experiments were carried out at 4, 25, and 60 °C with weight ratios between 0.02 and 1.4 g_{SO} g_{MNP}^{-1}, according to the conditions described in Table 1. The oleate quantification in the supernatant was performed with a modified RP-HPLC fatty acid analytic. The specific load of adsorbed oleate per unit mass of MNP was calculated from mass balance (Eq. 1) and transferred to the adsorption isotherms presented in Fig. 1:

$$q^* = (c - c^*)V/m_{\mathrm{MNP}} \quad (1)$$

Here q^* is the specific amount of adsorbed oleate species per unit mass of MNP, c is the total concentration of oleate molecules in the reaction volume V, c^* is the concentration of oleate molecules in the particle free supernatant (equilibrium concentration in solution), and m_{MNP} is the total mass of MNP in the system.

The results in Fig. 1 reveal a maximal specific load of oleate per unit mass MNPs to be in the range of 0.35–0.37 g_{oleate} g_{MNP}^{-1} for all temperatures investigated. The data for 60 °C fit well with the Langmuir adsorption model in Eq. 2, where K_L is the Langmuir adsorption coefficient and q^*_{max} is the maximal amount of adsorbed oleate per unit mass of MNP:

$$q^* = \frac{K_L q^*_{\mathrm{max}} c^*}{1 + K_L c^*}. \quad (2)$$

K_L was determined to 8.97 L g_{oleate}^{-1} and q^*_{max} to 0.40 g_{oleate} g_{MNP}^{-1}.

At 60 °C, the specific load remains at a constant level (saturation) with addition of SO after reaching q^*_{max}, whereas it tends to decrease for the samples T4 and T25. This tendency was reproduced in a validation experiment for T25 (valid. T25). Both behavior forms are described for similar systems where surface active agents in the presence of metal oxide surfaces in aqueous solutions were studied (Pagac et al. 1998). Nevertheless, the presence of maxima is still not well understood, and theories seeking to explain it have not been confirmed experimentally (Arnebrant et al. 1989; Paria et al. 2005).

As often discussed in the literature, surfactant organization in a given solid–liquid system depends primarily on the chemical nature of the surfactant, temperature, pH, and ionic strength (Kulkarni and Somasundaran 1980; Scamehorn et al. 1982; Somasundaran and Huang 2000). Nanoparticles affect the surface tension of the suspension as well as the critical micelle concentration, CMC of the surface active compound (Liu and Kai 2012; Lestari et al. 2015; Cerdeira et al. 2012), which in our case is oleate. The mechanisms of simultaneous adsorption and micelle formation are not fully understood nowadays, but the general approach is that adsorption on the nanoparticles surface competes with micellar formation only for high surfactant concentrations. This is strongly dependent on the system chosen and the conditions, but for oleate, it is generally accepted that the interaction between oleate and the iron oxide surface is stronger than the tendency to form micelles (Wooding et al. 1991): for lower concentration, the oleate is generally adsorbed or in solution; the micellar system starts forming only after a boundary concentration in solution has been reached. This is assuredly a dynamic process with continuous exchange of species between the oleate molecules of the different structural parts (adsorbed, dissolved and in micelles or smaller groups).

Figure 1 suggests a correlation between the adsorption behavior after saturation (q^*_{max}) and the CMC of oleate in aqueous solutions. The CMC of our oleate is 0.17 g_{oleate} L^{-1} as determined by tensiometry (see Fig. S1); this value increases with increasing temperature (Korolev et al. 2002; Klevens 1948). Beyond reaching the corresponding CMC, we expect that

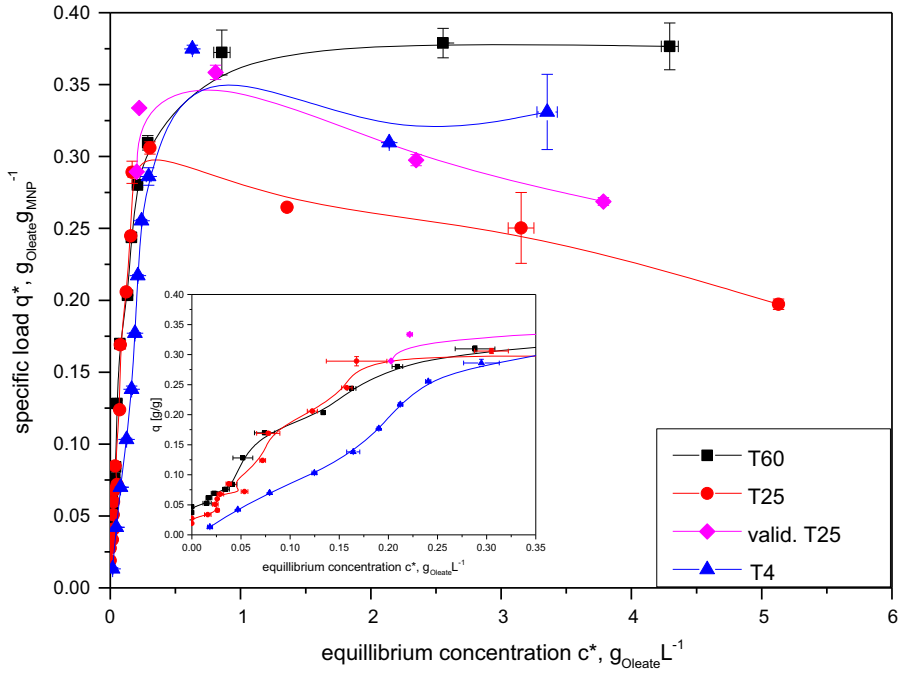

Fig. 1 Oleate adsorption isotherms on MNP prepared at 4, 25, and 60 °C with a close-up of the linear part. The specific amount of adsorbed oleate species per unit mass of MNP, q^* is plotted against the concentration of oleate molecules in the particle free supernatant, c^* (equilibrium concentration in solution). Data of "valid. T25" corresponds to the repetition of the experiments at 25 °C

further addition of oleate contributes to constant adsorption of oleate on the MNP surface and parallel formation of micellar structures. Therefore, the decrease of q^* at high values of c^* (for 4 and 25 °C) might be related to an exchange process between oleate species from the MNP double-layer and micellar structures of oleate in the supernatant. At the moment, we cannot explain why this behavior changes at higher temperatures; it might be related to a change in the CMC as well as to temperature effects on the suspension properties and the solubility of the species.

Based on the results for q^*_{max}, it is possible to calculate the maximal oleate bilayer packing density at the MNP surface. Peaks of all patterns had been successfully attributed to the Bragg positions of magnetite given by the JCPDS-International Center for Diffraction Data (JCPDS Card: 19-629), as displayed in Fig. 2. The particle size calculated with the Scherrer equation accounts for 10.0 nm.

The specific iron oxide surface was determined to be 98.4 ± 2.3 $m^2\ g^{-1}$ by N_2 adsorption isotherms with the BET method. From the specific oleate load per unit mass of MNP q^*, the Avogadro constant N_A, the molecular weight of oleate (M_{oleate} = 281.4 g mol^{-1}), and m_{MNP} (8.6 mg), we can calculate the number of oleate molecules n_{oleate} on the MNP surface applying Eq. (3):

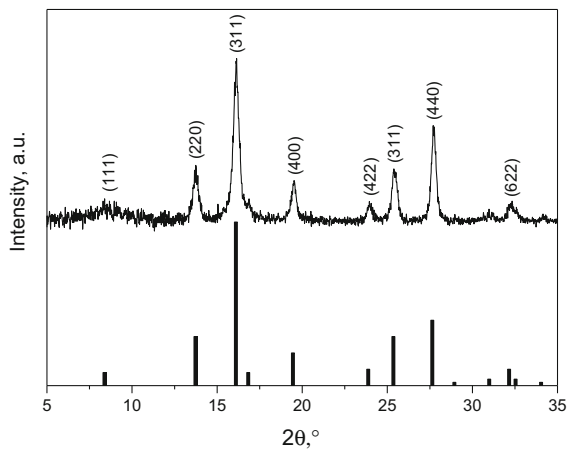

Fig. 2 XRD pattern and predicted Bragg reflex intensities

$$n_{oleate} = \frac{q^* m_{MNP}}{M_{oleate}} N_A \quad (3)$$

We calculate the space requirement A_{oleate} of an oleate molecule at the iron oxide surface by simplifying the system as a double-layer structure with the same surface coverage on both the inner and outer layers. For saturation conditions (q^*_{max} = 0.37 $g_{oleate}\ g^{-1}_{MNP}$), the resulting area of the head group on the iron oxide surface is calculated to approx. A_{oleate} = 25 $Å^2$. Wang et al. (Wang et al. 2013) had calculated an area

of 20 Å^2 for one molecule of oleate at the solid/water interface under CMC conditions, a value which corresponds closely with our results and demonstrates that in our system, the metal oxide surface should be completely saturated with a compact oleate bilayer. The area estimated is also very close to the average cross-sectional area of an alkyl-chain (18.8 Å^2) (Heinz et al. 2008). Data in the literature for water solutions of sodium oleate (without the presence of nanoparticles) yield values in a range from 26 Å^2 to more than 50 Å^2, depending on pH and temperature (Theander and Pugh 2001).

While temperature appears to have no significant influence on q^*_{max}, adsorption equilibrium at low ratios of SO/MNP is affected at low temperatures, as can be seen in the close-up of the linear part of the adsorption isotherms (Fig. 1). Compared to samples T25 and T60, the equilibrium concentration of oleate in the supernatant of sample T4 remains higher with the same oleate addition. This effect might be related to the fact that at low temperatures, the mobility of the oleate hydrocarbon backbone is reduced. Therefore, less interpenetration occurs between the oleate species from both layers, leading to a lower coverage of the layers.

Saturation magnetization measurements were carried out for the maximally loaded particles at 25 °C and showed very high saturation magnetization (>70 A m^2 kg^{-1}), close to values for particles synthesized through thermal decomposition (Moya et al. 2015). Our study, hence, demonstrates that the straightforward method of in situ precipitation and coating yields similar results to the ones from significantly more complicated methods, offering distinct advantages for industrially oriented applications.

Thermogravimetric analysis

In order to improve our understanding of the system, some of the samples which were coated at 60 °C (T60) were analyzed thermogravimetrically (Fig. 3). Components of thermal decomposition were monitored with a mass spectrometer, and the relative mass loss of the samples and the ion current for analyzed ratios of m z^{-1} are displayed in Fig. 3.

TGA curves show a weight loss in two temperature ranges, from 250 to 400 °C and from 600 to 720 °C. Results of mass spectrometry confirm that the mass loss in both temperature spans derive from oleate species (Fig. S3). The weight loss in the low-temperature region can be attributed to the desorption and decomposition of oleate molecules from the outer part of the lipid double layer, while the weight loss in the relatively high temperature region results from oxidative decomposition of oleate molecules which are chemisorbed on the MNP surface. The chemisorbed inner oleate layer, which is partially carbonized above 500 °C, is oxidatively decomposed from 600 to 720 °C which can be evidenced as strong CO_2 signal (m z^{-1} 44) in Fig. S3. The oxidation of the partially oxidized inner oleate layer is accompanied by a reduction of MNP to wüstite (Rudolph et al. 2012) which can be evidenced with XRD (Fig. S4). The detailed thermal decomposition of adsorbed oleate with intermediate stages is described in the supplementary material. These results support the double-layer theory of oleate coated MNP in aqueous solutions and are in agreement with other TGA data discussed in the literature (Huang et al. 2008; Jiang et al. 2010). The results also suggest that formation of a bilayer occurs already for low grades of oleate adsorption. Smaller specific loads of oleate on MNP demonstrate both chemisorbed and physisorbed oleate species, which decompose at 250–400 and 600–720 °C, respectively. Hence, the oleate adsorption onto the MNP surface may follow a quasi-first order kinetic mechanism forming small carpet-like double-layer islands rather than monolayers, as suggested by Wooding et al. (1991). With an increase of the equilibrium oleate concentration in the

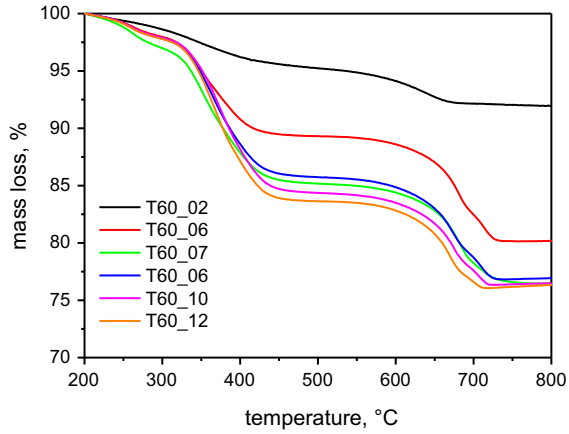

Fig. 3 Thermogravimetric analysis of samples from T60 with representation of percentual mass loss values

supernatant, the oleate islands start to expand (more oleate units) until they unite with other islands at the edges. This process continues, until the whole MNP surface is covered.

FT-IR

In addition to the TGA analysis, the sequential coating of MNP for assay T_60 was monitored with FT-IR. Therefore, all spectra were normalized to the Fe–O vibration at 577 cm^{-1} (Yang et al. 2010). SO was measured as a reference. Spectra are displayed in Fig. 4.

In Fig. 4, the strong bands at 2919 and 2850 cm^{-1} correspond to the asymmetric and symmetric stretch modes of ν (CH_2), respectively, while the deformation bands at 2960 and 2870 cm^{-1} derive from the asymmetric and symmetric stretch of ν (CH_3), respectively (Jovanović et al. 2014). The weak appearance can be attributed to the small ratio of CH_3 groups compared to CH_2 groups in the oleate molecule. The bands of symmetric deformation modes can be observed at 1460 and 1443 cm^{-1} for δ (CH_2) and at 1377 cm^{-1} for δ (CH_3). A weak band at 1654 cm^{-1} can be attributed to the stretch mode of ν (C=C) double bond in the oleate molecule, which is expected from 1660 to 1630 cm^{-1} for *cis* conformation (Nakamoto 2006). This band is partly overlapped by a δ (OH) bending mode appearing around 1632 cm^{-1} of adsorbed water. The difference in wave number (Δ) between the symmetric and asymmetric carboxylate stretch vibrations corresponding to bands at 1558 and 1423 cm^{-1}, respectively, indicates ionic carboxylate coordination in the SO reference. According to numerous studies, Δ is strongly dependent on the carboxylate coordination (Schwaminger et al. 2015; Jovanović et al. 2014; Nakamoto 2006; Bronstein et al. 2007).

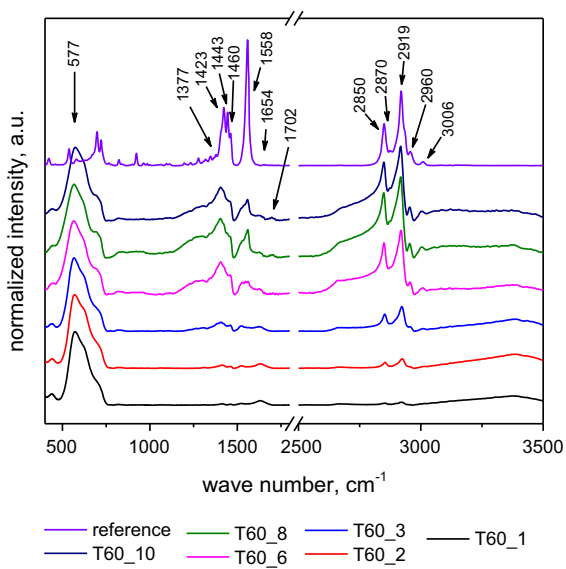

Fig. 4 FT-IR spectra of selected samples of T60 with SO as reference

Successful oleate coating of the MNP is confirmed by the existence of characteristic bands, matching the peaks of the SO reference. The increase in peak intensity with sample number indicates higher grades of oleate coating. A closer look at the asymmetric carboxylate stretch mode of the coated MNP reveals the existence of two states of coordination for the carboxylate groups. The peaks corresponding to symmetric carboxyl stretch vibrations appear at approximately 1530 and 1562 cm^{-1}. With the asymmetric carboxyl stretch band at 1402 cm^{-1}, Δ is calculated to 128 and 160 cm^{-1}, indicating the simultaneous presence of bidentate and ionic coordination of carboxylate groups, respectively (Roonasi and Holmgren 2009; Jiang et al. 2010; Jovanović et al. 2014). At low coating grades, the carboxylate coordination is primarily bidentate, while at higher grades, an ionic coordination of carboxyl groups appears in the IR spectra. Bidentate coordination is attributed to the carboxylate groups directly adsorbed on the iron oxide surface (Bronstein et al. 2007), while the ionic character is ascribed to carboxylic groups of oleate species from the secondary layer. The results indicate that for lower coating grades, the formation of the primary layer is promoted; at the same time, the secondary layer is loosely packed. The increase of the ionic character with sample number indicates a more dense packing of the secondary layer, which supports the data from the TGA measurements. At high sample numbers a band at 1702 cm^{-1} becomes visible, which can be attributed to the asymmetric stretch ν (C=O), known from dimeric carboxylic acids (Young et al. 2008). The symmetric stretch of dimeric acids, expected at 1660 cm^{-1} overlaps with the ν (C=C) stretch and the δ (O–H) bending mode (Nakamoto 2006). These data suggest the formation of dimers at the carboxylic head groups of the secondary layer at high concentrations of oleate molecules in aqueous phase.

Zeta potential

Electrostatic stabilization as a function of MNP coating was characterized by zeta potential measurements at 25 °C. Samples of experiments T25 were chosen for characterization in order to exclude temperature influence on oleate load. The change in zeta potential with pH is illustrated in Fig. 5.

The stepwise stabilization of MNP with SO can be monitored by the change in surface charge (Fig. 5), corresponding to the negatively charged carboxylic head groups in the secondary lipid layer. For nanoscale magnetite particles, zeta potential ζ is described by a characteristically shaped sigmoid curve over pH with the isoelectric point at about pH 6.8–7.1 (Blesa et al. 1984; Massart 1981), which is in compliance with measured data. Recorded values for ζ range from $\zeta = -30$ mV at pH 10 to $\zeta = +40$ mV at pH 3. Coated samples show evidence of a drop in ζ to about $\zeta = -35$ mV at pH 10 and $\zeta = +5$ mV at pH 3; this demonstrates that the carboxylic groups at the outer surface of the lipid double layer are deprotonated over a wide pH range. Due to oleate coating of MNP, the isoelectric point is shifted to pH 4.3, which is in accordance with data from the literature (de Palma et al. 2007). Absolute values of $\zeta \geq 30$ mV are regarded as physically stable (Müller and Mehnert 1997); accordingly, the stabilizing effect of oleate coating on MNP in this study is achieved for $6 > \text{pH} > 10$ for higher oleate concentrations. Furthermore, the gradual change in ζ with the oleate coating grade indicates a transition stage between the iron oxide surface and the fully oleate coated surface. This effect can be explained by the formation of oleate islands, where the zeta potential is determined by the amphiphilic MNP surface and negatively charged carboxylic head groups. Similar results were previously obtained by Ramimoghadam et al. (2015b) for different adsorbed masses of dodecanoic acid on iron oxide nanoparticles.

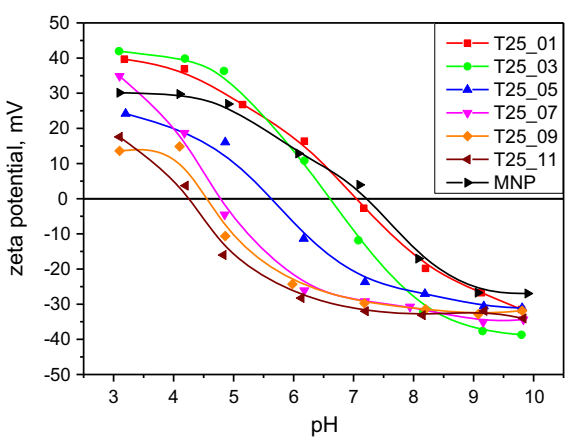

Fig. 5 Zeta potential of sample T25 from pH 3 to 10

Conclusion

We present a study of the adsorption process of sodium oleate on nanoscale superparamagnetic iron oxide nanoparticles in an aqueous medium. The focus of this work lies on the influence of temperature on the adsorption equilibrium to help better understand the adsorption mechanism of the oleate molecules on the surface of MNPs. The temperature variation does not appear to significantly influence values of the maximal specific load per unit mass of MNP (approx. 0.35 $g_{oleate}\ g_{MNP}^{-1}$). However, at low temperatures and high oleate concentrations in the supernatant a decrease of load is observed, possibly due to the simultaneous existence of micelles. From the measurements of the supernatant using RP-HPLC adsorption isotherms could be represented. FT-IR spectroscopy reveals a deeper insight into the formation process of the surfactant double layer as well as the success of the coating process. These results together with the thermogravimetric analysis of the residues suggest a quasi-first order adsorption mechanism of oleate molecules on the MNP surface, with the formation of carpet-like oleate islands with a double-layer structure. The data obtained provide information about the packing density of the oleate molecules in the primary and secondary layers, which are functions of the thermodynamic equilibrium between adsorbed oleate molecules and molecules in solution. Furthermore, formation of multilayers by dimerization of carboxylic groups can be observed at high concentrations of oleate species in the liquid phase. Changes in the zeta potential, which are related to a change in the surface charge, demonstrate the stabilizing effect of SO on aqueous MNP suspensions. As a result of the MNPs surface coverage with carboxylic groups, the isoelectric point shifted from approximately pH 7.4–4.3 for high oleate loads,

reducing the tendency to agglomerate over a broad pH range.

Our study shows the dynamic nature of surfactant adsorption on metal oxide surfaces. The complexity of the system makes this topic worthy of future research. To better understand adsorption mechanisms of surface active agents on magnetic nanoparticles, a comparison of the behavior of the system in relation to surface tension and adsorption capacity with and without nanoparticles under the same experimental conditions is required. Such studies are of great importance for a more effective application of adsorption as a separation, recovery, or removal tool in many research areas, e.g., pharmaceuticals, biochemistry, biotechnology, and environmental sciences as well as for further development of coating and adhesion processes.

Acknowledgments The authors would like to gratefully thank Prof. Dr. T. Nilges (Technical University of Munich) for his support with powder XRD and Stefan Heissler (Karlsruhe Institute of Technology, Institute of Functional Interfaces, Germany) for help with FT-IR measurements. Special gratitude is expressed to Martina Haack (Technical University of Munich, Industrial Biocatalysis Group, Germany) for performing gas chromatographic analysis. Furthermore, we would like to express our appreciation to Jonathan Ritscher for conducting part of the work in the context of student research projects. Additionally, we want to acknowledge the support of the TUM Graduate School, Technical University of Munich. We are particularly grateful for the financial support of this work by the Bavarian Ministry of Economic Affairs and Media, Energy and Technology (grant number 1340/68351/3/11), the Ministry of Education and Research (Grant number 031A173A) and Clariant.

References

Arnebrant T, Bäckström K, Jönsson B, Nylander T (1989) An ellipsometry study of ionic surfactant adsorption on chromium surfaces. J Colloid Interface Sci 128(2):303–312. doi:10.1016/0021-9797(89)90344-5

Balmasova OV, Korolev VV, Yashkova VI (2010) Oleic acid adsorption–desorption isotherms on the surface of high-dispersity ferrites from a solution in carbon tetrachloride. Russ J Phys Chem 84(1):76–80. doi:10.1134/S0036024410010152

Bao Y, Wen T, Samia ACS, Khandhar A, Krishnan KM (2016) Magnetic nanoparticles: material engineering and emerging applications in lithography and biomedicine. J Mater Sci 51(1):513–553. doi:10.1007/s10853-015-9324-2

Berensmeier S (2006) Magnetic particles for the separation and purification of nucleic acids. Appl Microbiol Biotechnol 73(3):495–504. doi:10.1007/s00253-006-0675-0

Blesa MA, Figliolia NM, Maroto AJG, Regazzoni AE (1984) The influence of temperature on the interface magnetite–aqueous electrolyte solution. J Colloid Interface Sci 101(2):410–418. doi:10.1016/0021-9797(84)90052-3

Bloemen M, Brullot W, Luong TT, Geukens N, Gils A, Verbiest T (2012) Improved functionalization of oleic acid-coated iron oxide nanoparticles for biomedical applications. J Nanopart Res 14(9):1–10. doi:10.1007/s11051-012-1100-5

Brandt A, Balducci A (2013) A study about the use of carbon coated iron oxide-based electrodes in lithium-ion capacitors. Electrochim Acta 108:219–225. doi:10.1016/j.electacta.2013.06.076

Bronstein LM, Huang XL, Retrum J, Schmucker A, Pink M, Stein BD, Dragnea B (2007) Influence of iron oleate complex structure on iron oxide nanoparticle formation. Chem Mater 19(15):3624–3632. doi:10.1021/Cm062948j

Cerdeira AM, Werner IA, Mazzotti M, Gander B (2012) Simultaneous quantification of polymeric and surface active stabilizers of nanosuspensions by using near-infrared spectroscopy. Drug Dev Ind Pharm 38(11):1360–1370. doi:10.3109/03639045.2011.650864

Chen MJ, Shen H, Li X, Liu HF (2014) Facile synthesis of oil-soluble Fe_3O_4 nanoparticles based on a phase transfer mechanism. Appl Surf Sci 307:306–310. doi:10.1016/j.apsusc.2014.04.031

Chin AB, Yaacob II (2007) Synthesis and characterization of magnetic iron oxide nanoparticles via w/o microemulsion and Massart's procedure. J Mater Process Technol 191(1–3):235–237. doi:10.1016/j.jmatprotec.2007.03.011

de Palma R, Peeters S, van Bael MJ, van den Rul H, Bonroy K, Laureyn W, Mullens J, Borghs G, Maes G (2007) Silane ligand exchange to make hydrophobic superparamagnetic nanoparticles water-dispersible. Chem Mater 19(7):1821–1831. doi:10.1021/Cm0628000

Griffiths MJ, van Hille RP, Harrison STL (2010) Selection of direct transesterification as the preferred method for assay of fatty acid content of microalgae. Lipids 45(11):1053–1060. doi:10.1007/s11745-010-3468-2

Heinz H, Vaia RA, Farmer BL (2008) Relation between packing density and thermal transitions of alkyl chains on layered silicate and metal surfaces. Langmuir 24(8):3727–3733. doi:10.1021/La703019e

Holčapek M, Jandera P, Fischer J, Prokeš B (1999) Analytical monitoring of the production of biodiesel by high-performance liquid chromatography with various detection methods. J Chromatogr A 858(1):13–31. doi:10.1016/S0021-9673(99)00790-6

Huang JH, Parab HJ, Liu RS, Lai TC, Hsiao M, Chen CH, Sheu HS, Chen JM, Tsai DP, Hwu YK (2008) Investigation of the growth mechanism of iron oxide nanoparticles via a seed-mediated method and its cytotoxicity studies. J Phys Chem C 112(40):15684–15690. doi:10.1021/Jp803452j

Jiang W, Wu Y, He B, Zeng X, Lai K, Gu Z (2010) Effect of sodium oleate as a buffer on the synthesis of superparamagnetic magnetite colloids. J Colloid Interface Sci 347(1):1–7. doi:10.1016/j.jcis.2010.02.055

Jovanović S, Spreitzer M, Tramšek M, Trontelj Z, Suvorov D (2014) Effect of oleic acid concentration on the physicochemical properties of cobalt ferrite nanoparticles. J Phys Chem C 118(25):13844–13856. doi:10.1021/jp500578f

Khalafalla SE, Reimers GW (1980) Preparation of dilution-stable aqueous magnetic fluids. Magn IEEE Trans 16(2):178–183. doi:10.1109/Tmag.1980.1060578

Kim DK, Zhang Y, Voit W, Rao KV, Muhammed M (2001) Synthesis and characterization of surfactant-coated superparamagnetic monodispersed iron oxide nanoparticles. J Magn Magn Mater 225(1–2):30–36. doi:10.1016/S0304-8853(00)01224-5

Klevens HB (1948) Critical micelle concentrations as determined by refraction. J Phys Colloid Chem 52(1):130–148. doi:10.1021/j150457a013

Korolev VV, Ramazanova AG, Blinov AV (2002) Adsorption of surfactants on superfine magnetite. Russ Chem Bull 51(11):2044–2049. doi:10.1023/A:1021655708965

Korolev VV, Blinov AV, Ramazanova AG (2004) Adsorption of fatty acids from solutions in organic solvents on the surface of finely dispersed magnetite: 2. Heats of oleic, linoleic, and linolenic acid adsorption from carbon tetrachloride and hexane. Colloid J 66(6):705–708. doi:10.1007/s10595-005-0058-8

Korolev VV, Balmasova OV, Ramazanova AG (2009) The sorption isotherms of oleic, linoleic, and linolenic acids from solutions in cyclohexane and heptane on magnetite. Russ J Phys Chem 83(6):1018–1021. doi:10.1134/S0036024409060259

Kulkarni RD, Somasundaran P (1980) Flotation chemistry of hematite/oleate system. Colloids Surf 1(3–4):387–405. doi:10.1016/0166-6622(80)80025-4

Laurent S, Forge D, Port M, Roch A, Robic C, Vander Elst L, Muller RN (2008) Magnetic iron oxide nanoparticles: synthesis, stabilization, vectorization, physicochemical characterizations, and biological applications. Chem Rev 108(6):2064–2110. doi:10.1021/cr068445e

Lestari MLAD, Müller RH, Möschwitzer JP (2015) Systematic screening of different surface modifiers for the production of physically stable nanosuspensions. J Pharm Sci 104(3):1128–1140. doi:10.1002/jps.24266

Liu Y, Kai D (2012) Investigations of surface tension of binary nanofluids. Adv Mater Res 347–353:786–790. doi:10.4028/www.scientific.net/AMR.347-353.786

Martínez-Mera I, Espinosa-Pesqueira ME, Pérez-Hernández R, Arenas-Alatorre J (2007) Synthesis of magnetite (Fe3O4) nanoparticles without surfactants at room temperature. Mater Lett 61(23–24):4447–4451. doi:10.1016/j.matlet.2007.02.018

Massart R (1981) Preparation of aqueous magnetic liquids in alkaline and acidic media. Magn IEEE Trans 17(2):1247–1248. doi:10.1109/TMAG.1981.1061188

Moya C, Batlle X, Labarta A (2015) The effect of oleic acid on the synthesis of Fe_3–xO_4 nanoparticles over a wide size range. Phys Chem Chem Phys. doi:10.1039/c5cp03395k

Müller RH, Mehnert W (1997) Particle and surface characterisation methods. Wissenschaftliche Verlagsgesellschaft, Stuttgart

Nakamoto K (2006) Infrared and Raman spectra of inorganic and coordination compounds. In: Chalmers JM, Griffiths PR (eds) Handbook of vibrational spectroscopy. Wiley, New York. doi:10.1002/0470027320.s4104

Norlén L, Nicander I, Lundsjö A, Cronholm T, Forslind B (1998) A new HPLC-based method for the quantitative analysis of inner stratum corneum lipids with special reference to the free fatty acid fraction. Arch Dermatol Res 290(9):508–516. doi:10.1007/s004030050344

Pagac ES, Prieve DC, Tilton RD (1998) Kinetics and mechanism of cationic surfactant adsorption and coadsorption with cationic polyelectrolytes at the silica–water interface. Langmuir 14(9):2333–2342. doi:10.1021/LA971308F

Paria S, Khilar KC (2004) A review on experimental studies of surfactant adsorption at the hydrophilic solid–water interface. Adv Colloid Interface Sci 110(3):75–95. doi:10.1016/j.cis.2004.03.001

Paria S, Manohar C, Khilar KC (2005) Adsorption of anionic and non-ionic surfactants on a cellulosic surface. Colloids Surf A 252(2):221–229. doi:10.1016/j.colsurfa.2004.09.022

Park J, An K, Hwang Y, Park J-G, Noh H-J, Kim J-Y, Park J-H, Hwang N-M, Hyeon T (2004) Ultra-large-scale syntheses of monodisperse nanocrystals. Nat Mater 3(12):891–895. doi:10.1038/nmat1251gac

Ramimoghadam D, Bagheri S, Abd Hamid SB (2015a) Stable monodisperse nanomagnetic colloidal suspensions: an overview. Colloids Surf B. doi:10.1016/j.colsurfb.2015.02.003

Ramimoghadam D, Bagheri S, Hamid SBA (2015b) In-situ precipitation of ultra-stable nano-magnetite slurry. J Magn Magn Mater 379:74–79. doi:10.1016/j.jmmm.2014.12.005

Ramos-González R, García-Cerda LA, Quevedo-López MA (2012) Study of the surface modification with oleic acid of nanosized HfO_2 synthesized by the polymerized complex derived sol–gel method. Appl Surf Sci 258(16):6034–6039. doi:10.1016/j.apsusc.2012.02.122

Reddy LH, Arias JL, Nicolas J, Couvreur P (2012) Magnetic nanoparticles: design and characterization, toxicity and biocompatibility, pharmaceutical and biomedical applications. Chem Rev 112(11):5818–5878. doi:10.1021/cr300068p

Roonasi P, Holmgren A (2009) A Fourier transform infrared (FTIR) and thermogravimetric analysis (TGA) study of oleate adsorbed on magnetite nano-particle surface. Appl Surf Sci 255(11):5891–5895. doi:10.1016/j.apsusc.2009.01.031

Roonasi P, Yang XF, Holmgren A (2010) Competition between sodium oleate and sodium silicate for a silicate/oleate modified magnetite surface studied by in situ ATR-FTIR spectroscopy. J Colloid Interface Sci 343(2):546–552. doi:10.1016/j.jcis.2009.12.002

Roth H-C, Schwaminger SP, Schindler M, Wagner FE, Berensmeier S (2015) Influencing factors in the co-precipitation process of superparamagnetic iron oxide nano particles: a model based study. J Magn Magn Mater 377:81–89. doi:10.1016/j.jmmm.2014.10.074

Rudolph M, Erler J, Peuker UA (2012) A TGA-FTIR perspective of fatty acid adsorbed on magnetite nanoparticles-decomposition steps and magnetite reduction. Colloids Surf A 397:16–23. doi:10.1016/j.colsurfa.2012.01.020

Scamehorn J, Schechter R, Wade W (1982) Adsorption of surfactants on mineral oxide surfaces from aqueous solutions: I: isomerically pure anionic surfactants. J Colloid Interface Sci 85(2):463–478. doi:10.1016/0021-9797(82)90013-3

Schilt AA (1969) Analytical applications of 1, 10-phenanthroline and related compounds, vol 32, 1st edn., International series of monographs in analytical chemistryPergamon Press, New York

Schwaminger SP, Fraga García P, Merck GK, Bodensteiner FA, Heissler S, Günther S, Berensmeier S (2015) Nature of interactions of amino acids with bare magnetite nanoparticles. J Phys Chem C 119(40):23032–23041. doi:10.1021/acs.jpcc.5b07195

Somasundaran P, Huang L (2000) Adsorption/aggregation of surfactants and their mixtures at solid–liquid interfaces. Adv Colloid Interface Sci 88(1):179–208. doi:10.1016/S0001-8686(00)00044-0

Theander K, Pugh RJ (2001) The Influence of pH and temperature on the equilibrium and dynamic surface tension of aqueous solutions of sodium oleate. J Colloid Interface Sci 239(1):209–216. doi:10.1006/jcis.2000.7543

Wang Y, Wong JF, Teng XW, Lin XZ, Yang H (2003) "Pulling" nanoparticles into water: phase transfer of oleic acid stabilized monodisperse nanoparticles into aqueous solutions of α-cyclodextrin. Nano Lett 3(11):1555–1559. doi:10.1021/Nl034731j

Wang C, Zhao X, Zhao J, Liu Y, Sheng Y, Wang Z (2007a) Biomimetic nucleation and growth of hydrophobic vaterite nanoparticles with oleic acid in a methanol solution. Appl Surf Sci 253(10):4768–4772. doi:10.1016/j.apsusc.2006.10.048

Wang X, Zhang C, Wang X, Gu H (2007b) The study on magnetite particles coated with bilayer surfactants. Appl Surf Sci 253(18):7516–7521. doi:10.1016/j.apsusc.2007.03.053

Wang Z, Lam A, Acosta E (2013) Suspensions of Iron oxide nanoparticles stabilized by anionic surfactants. J Surf Deterg 16(3):397–407. doi:10.1007/s11743-012-1425-1

Wooding A, Kilner M, Lambrick DB (1991) Studies of the double surfactant layer stabilization of water-based magnetic fluids. J Colloid Interface Sci 144(1):236–242. doi:10.1016/0021-9797(91)90254-6

Yan F, Li J, Zhang J, Liu F, Yang W (2009) Preparation of Fe_3O_4/polystyrene composite particles from monolayer oleic acid modified Fe_3O_4 nanoparticles via miniemulsion polymerization. J Nanopart Res 11(2):289–296. doi:10.1007/s11051-008-9382-3

Yang K, Peng H, Wen Y, Li N (2010) Re-examination of characteristic FTIR spectrum of secondary layer in bilayer oleic acid-coated Fe_3O_4 nanoparticles. Appl Surf Sci 256(10):3093–3097. doi:10.1016/j.apsusc.2009.11.079

Young AG, Al-Salim N, Green DP, McQuillan AJ (2008) Attenuated total reflection infrared studies of oleate and trioctylphosphine oxide ligand adsorption and exchange reactions on CdS quantum dot films. Langmuir 24(8):3841–3849. doi:10.1021/La703655v

Zhang L, He R, Gu HC (2006) Oleic acid coating on the monodisperse magnetite nanoparticles. Appl Surf Sci 253(5):2611–2617. doi:10.1016/j.apsusc.2006.05.023

Zhou X, Ni S, Wang X, Wu F (2007) Adsorption of sodium oleate on nano-sized fe_3o_4 particles prepared by coprecipitation. Curr Nanosci 3(3):259–263. doi:10.2174/157341307781422942